Light Emission in Silicon from Carbon Nanotubes

Etienne Gaufrès,[†] Nicolas Izard,[*] Adrien Noury, Xavier Le Roux, Gilles Rasigade, Alexandre Beck, and Laurent Vivien[*]

Institut d'Electronique Fondamentale, CNRS-UMR 8622, Univ. Paris Sud, Orsay, France. [†]Present address: Martel group, Univ. Montréal, Montréal, Canada.

ABSTRACT

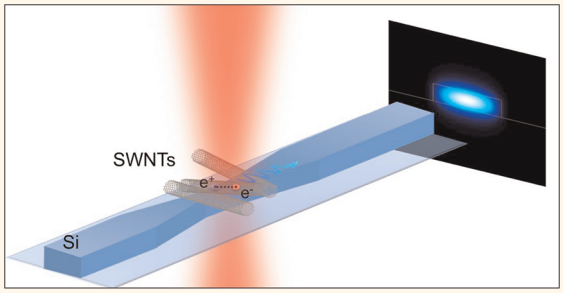

The use of optics in microelectronic circuits to overcome the limitation of metallic interconnects is more and more considered as a viable solution. Among future silicon compatible materials, carbon nanotubes are promising candidates thanks to their ability to emit, modulate, and detect light in the wavelength range of silicon transparency. We report the first integration of carbon nanotubes with silicon waveguides, successfully coupling their emission and absorption properties. A complete study of this coupling between carbon nanotubes and silicon waveguides was carried out, which led to the demonstration of the temperature-independent emission from carbon nanotubes in silicon at a wavelength of 1.3 μm. This represents the first milestone in the development of photonics based on carbon nanotubes on silicon.

KEYWORDS: nanotube · photonics · silicon · photoluminescence

Enhancing microprocessor performances is becoming increasingly more complex. This complexity stems from the rising transistor count and the transistor's shrinking size in the quest to follow Moore's Law.[1] As a consequence, power consumption in microprocessor increases, and the on-chip communication between different components becomes more and more difficult and is even now a key-point for future multicore generations.[2] To overcome these problems, one of the most promising solutions is the use of optical interconnects, which combine high data rate transmission, low power consumption, synchronization, and crosstalk.[3,4] In recent years, silicon photonics was extensively studied for the realization of high-speed optical links.[5−7] Nowadays, compact photonic structures are achieved due to the strong refractive index contrast between silicon and silica and low loss optical propagation in the wavelength range from 1.25 to 1.65 μm. In particular, various passive devices for wavelength multiplexing or light distribution (90° bends) are easily feasible with silicon photonics technology.[8,9]

Nevertheless, silicon is an indirect band gap material, and its optoelectronic properties are insufficient to generate light and not sensitive enough to detect the flux of photons transmitted in an optical link. Other materials, such as III−V semiconductors, are good alternatives for light emission,[10,11] while germanium could realize high-speed photodetectors.[12,13] Silicon is still used for efficient and high speed optical modulators.[14] The integration of all of these materials on silicon is technically possible, but as different and sometimes noncompatible processes are used, the resulting scheme is not cost-effective and consequently reduces the use of silicon photonics for a broad application domain. A monolithic integration of laser source, optical modulator, and photodetector with a common material would be much more favorable for emergence of photonics.

We envision the use of carbon nanotubes for all active optoelectronic devices in silicon in order to avoid these noncompatible processes. Carbon nanotubes (SWNTs) are a very versatile material, presenting at the same time very good electronic properties[15] and optical properties.[16−18] They display strong photo- and electroluminescence, in the 1−2 μm wavelength range,[19−22] and the emission could be tuned by selecting a precise nanotube diameter and chirality.[23] The possibility to use electrical pumping for luminescence generation is extremely interesting for the realization of an electrically pumped optical laser.[24,25] Recent works revealed that SWNTs display electroabsorption

* Address correspondence to nicolas.izard@u-psud.fr, laurent.vivien@u-psud.fr.

Received for review December 16, 2011 and accepted April 25, 2012.

Published online April 25, 2012
10.1021/nn204924n

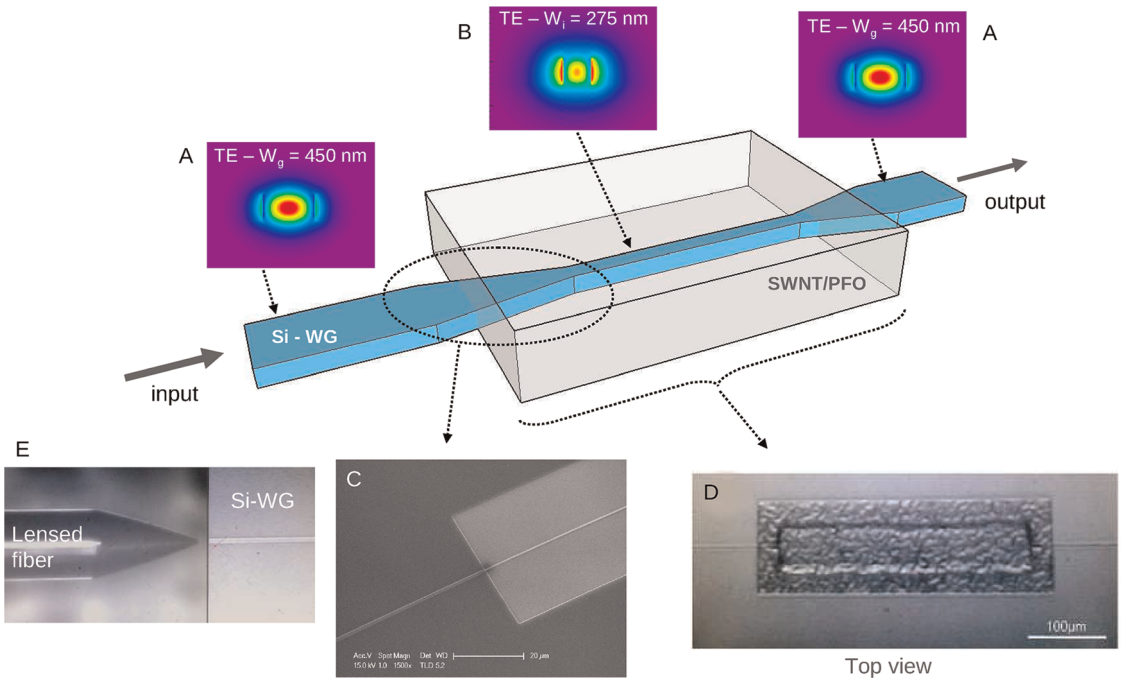

Figure 1. Integration scheme of carbon nanotube thin layer composite with silicon waveguide. (A) Input and output single-mode silicon waveguides with a height of 220 nm and a width W_g of 450 nm. The optical mode for TE polarization is strongly confined into the silicon waveguide. (B) Interaction region with carbon nanotubes and the silicon waveguide, with a height of 220 nm and a width W_i of 275 nm. The guided mode is deconfined, and a significant fraction of the energy propagates outside the waveguide. (C) SEM view of the adiabatic taper, which adapts the mode from the input waveguide (W_g) to the interaction zone waveguide (W_i). (D) Optical microscope top view of the final device, with the silica recess and SWNT/PFO thin layer on top of it. The apparent roughness on top of the SWNT/PFO thin film is due to the low-temperature SiO_2 hard mask used in the last technological step. (E) Optical microscope view of the lensed fiber used to inject the input light into the cleaved waveguide facet.

properties, which could be used to achieve optical modulation.[26,27] Finally, nanotubes present various absorption bands in the 1−2 μm range, allowing realization of photodetectors.[28,29] Therefore, carbon nanotubes are very good candidates to solve integration issues in silicon photonics and make cost-effective and reliable photonics. Moreover, a side advantage of the use of nanotubes for photonics is that the current research on the use of nanotubes for nanoelectronics[30] will facilitate the integration between photonics and electronics.

In this paper, we propose a way to integrate nanotubes with silicon photonics technology, which is a key-point for future realization of carbon-nanotube-based photonic devices. This work looks into the difficulties of coupling the optical properties of a 1D nanomaterial (SWNT) to a bulk 3D material such as silicon. In this context, we report the first integration of nanotubes' absorption and emission properties in silicon waveguides at telecommunication wavelengths around 1.3 μm.

RESULTS AND DISCUSSION

Integration Scheme Design. The integration scheme considered is based on the insertion of an interacting zone in an input/output silicon waveguide. It is constituted of a submicrometer silicon waveguide embedded in a carbon nanotube composite, as schematically presented in Figure 1. The input and output waveguides have a width W_g of 450 nm. For such geometry, the optical mode is strongly confined into the waveguide (Figure 1A) due to the high refractive index contrast between silicon (optical index 3.45) and its top and bottom cladding layers where the index is near 1.45. This confinement prevents strong interactions with the surrounding media, allowing high transmission of optical signal. On the other hand, the waveguide in the interaction region with carbon nanotubes has a width W_i below the critical minimum confinement width W_c, which is the limit where a significant fraction of the optical mode starts to leak outside the silicon waveguide. At 1.3 μm, W_c is around 400 nm. A judicious shrinkage of the waveguide width W_i allows both deconfining a controlled fraction of the optical mode and preserving the propagation of the optical wave along the waveguide. Figure 1B illustrates the mode confinement calculated for a W_i of 275 nm and shows the optical mode spreading outside the waveguide silicon core. As a significant fraction of the energy is propagating outside the waveguide, the guided mode will have a strong interaction with the active SWNT-based polymer top cladding layer. To minimize optical losses in the transition between the input/output waveguide (W_g = 450 nm) and the

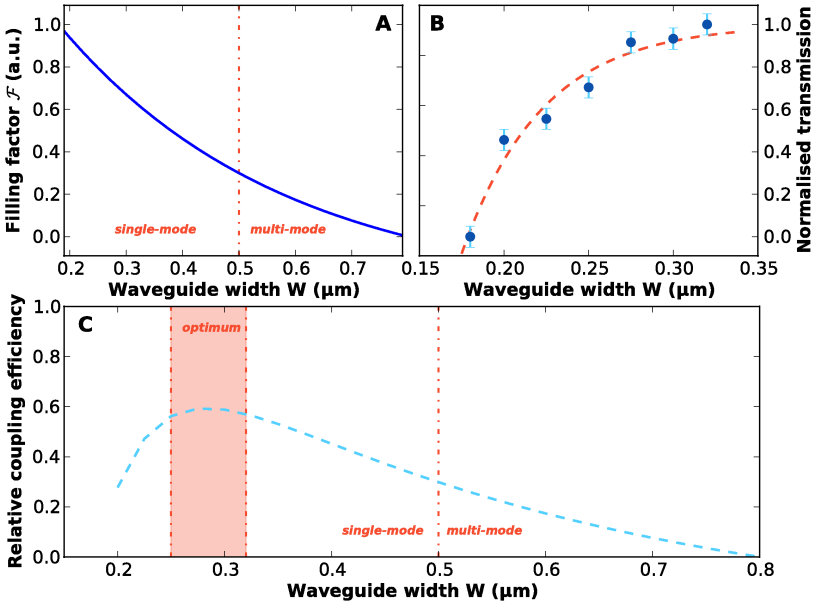

Figure 2. Determination of the waveguide width *W* to optimize the interaction between the optical mode in the silicon waveguide and carbon nanotubes. (A) Simulation of the evolution of the optical mode fraction confined in the SWNT/PFO layer (filling factor $\mathcal{F}$) as a function of the silicon waveguide width *W*. (B) Experimental results of the normalized transmission as a function of the silicon waveguide width *W*. (C) Optimal conditions which fulfill low loss and strong interaction of the optical modes with SWNTs. This results from the convolution of (A) and (B). The optimum waveguide width range is between 250 and 330 nm.

interaction region waveguide (W_i = 275 nm), adiabatic tapers are required (typically 300 μm long).

Technology. The substrate is a silicon-on-insulator (SOI) with a 220 nm thick silicon layer on top of a 1 μm thick buried silica layer. Although details of the technological steps are given in Supporting Information, briefly, silicon waveguides were made using e-beam lithography patterning followed by reactive ion plasma etching (RIE). A 500 nm thick silicon dioxide (SiO_2) protection layer was deposited onto the silicon wafer using a plasma-enhanced chemical vapor deposition (PECVD) technique. A silica recess of length *L* corresponding to the interaction region was etched down to the buried silicon oxide layer in order to expose the vicinity of the waveguide allowing interactions with the surrounding medium, in particular SWNT (Figure 1C).

The single-walled carbon nanotube (SWNT) film was prepared as follows: as-prepared HiPCO SWNT powder (Unydim Inc.) was mixed with poly-9,9-di-*n*-octylfluorenyl-2,7-diyl (PFO) in toluene in a ratio of SWNT (5 mg)/PFO (5 mg)/toluene (30 mL). This mixture was homogenized by sonication (for 1 h using a water-bath sonicator and 15 min using a tip sonicator) and was centrifuged for 5−60 min using a desktop centrifuge (angle rotor type, 10 000*g*). Solution was then drop casted directly into the previously defined silica recess to form a 1 μm thick layer. Samples were further annealed at 180 °C for 15 min to improve optical quality of the SWNT/PFO film.[19,31] This layer was then delimited around the interaction region by another O_2-based RIE to remove the SWNT/PFO film on the undesired areas (Figure 1D).

The evolution of the optical mode fraction confined in the SWNT/PFO layer (filling factor $\mathcal{F}$) was determined as a function of the waveguide width *W* by mode-solving numerical simulations using an home-made simulation code and is displayed in Figure 2A. The multimode/single-mode limit is found to be around 500 nm. As *W* narrows down, the filling factor (*i.e.*, the amount of energy in the SWNT/PFO layer) increases, thus strengthening the optical mode interaction with carbon nanotubes. Ideally, the waveguide width *W* should be reduced down to 150 nm and even less to optimize light interaction with the SWNT. However, silicon waveguides are on top of a 1 μm thick SiO_2 layer. If the optical mode transmitted into the waveguide is too deconfined, it will start to leak through the SiO_2 layer toward the silicon substrate, resulting in huge losses. Figure 2B displays experimental transmission results performed on optical waveguide of the same length with several width *W*. As *W* is reduced, the optical transmission through the waveguide exponentially decreases.

There is an optimum for a waveguide width to fulfill both high transmission and strong interactions with the SWNT/PFO layer. This optimum could be determined thanks to the convolution of the experimental transmission and the simulated filling factor. The obtained result is displayed in Figure 2C. The optimum waveguide width *W* was found to be between 250 and 330 nm. Consequently, a waveguide width W_i of 275 nm was used for the interaction region.

Absorption Coupling. The integration of SWNTs in silicon and the coupling of their optical properties

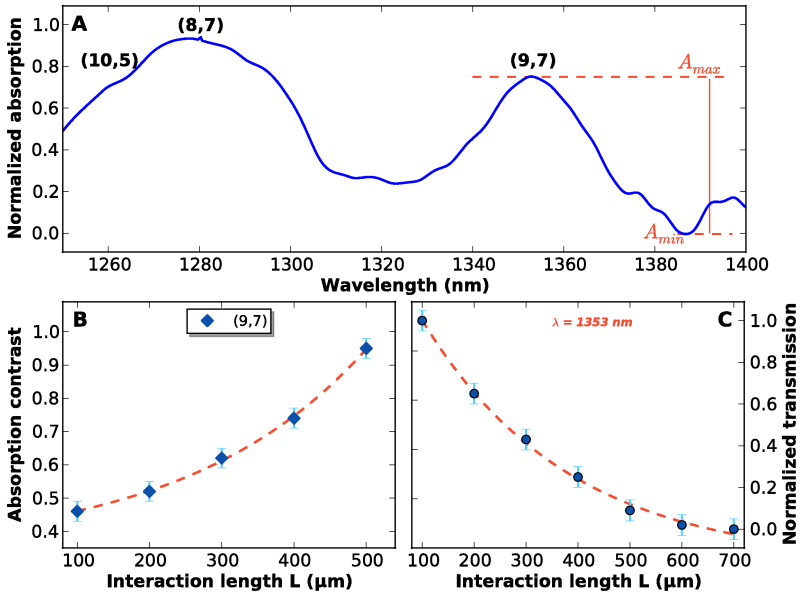

Figure 3. Carbon nanotube absorption measurements in the silicon waveguide. Evolution with the interaction length *L*. (A) Normalized absorption as a function of wavelength from 1250 to 1400 nm. The (10,5), (8,7), and (9,7) species are clearly observed. (B) Absorption contract *C* of the (9,7) nanotube, defined by $(A_{max} - A_{min})/(A_{max} + A_{min})$ as a function of the interaction length *L*. (C) Normalized transmission of the (9,7) nanotube at $\lambda = 1353$ nm as a function of the interaction length *L*.

were first demonstrated by measuring the absorption of the upper SWNT/PFO layer across the waveguide. A laser beam from a tunable fibered laser source with an emission wavelength centered at 1.3 μm was used at TE polarization (*i.e.*, electric field parallel to the substrate). Input light was injected into the cleaved waveguide facet using a lensed fiber (Figure 1E). A liquid nitrogen cooled InGaAs monocanal detector recorded the output beam through a monochromator.

Figure 3A reports the absorption spectrum of the carbon nanotubes through the silicon waveguide. In this case, the waveguide width W_i and length *L* in the interaction region were 275 nm and 400 μm, respectively. Several absorption peaks could be observed, each one corresponding to the specific absorption of one kind of nanotubes with specific (*n*,*m*) index. In the considered wavelength range (1.25−1.4 μm), three different SWNTs are clearly identified, corresponding to (10,5), (8,7), and (9,7) indexes.

The influence of the interaction length *L* was studied from the absorption contrast *C* of the (9,7) SWNT defined as

$$C = \frac{A_{max} - A_{min}}{A_{max} + A_{min}} \quad (1)$$

where A_{max} and A_{min} are, respectively, the maximum and minimum absorption of the (9,7) absorption peak, as defined in Figure 3A.

Both the absorption contrast and the output intensity level were determined for several waveguide interaction lengths *L*, increasing from 100 to 500 μm. Results are displayed in panels B and C of Figure 3, respectively. For the same waveguide width W_i of 275 nm, the absorption contrast *C* increases when *L* increases. On the same time, we found out that the waveguide transmission at $\lambda = 1353$ nm (corresponding to the absorption peak of the (9,7) nanotube) is decreasing when *L* increases. Both results follow a Beer−Lambert-type exponential law, indicating that the nature of the interaction between the optical mode propagated through the waveguide and carbon nanotubes is, indeed, optical absorption and not diffusive in nature. This result is the first signature of an effective coupling between SWNT absorption and the optical mode transmitted by the silicon waveguide.

Considering integration of carbon nanotubes with future photonic devices, there is a trade-off between the interaction with nanotubes (absorption contrast) and the waveguide transmission level. Several figures of merit could be proposed depending on the relative weight between absorption contrast and the global transmission of the device; however, an optimum interaction length L_i would be in the range of 400−500 μm, leading to very compact and low loss SWNT-based photonic devices.

Light Emission. In order to investigate whether or not the proposed integration scheme is promising for carbon-nanotube-based optical sources, the light emission from SWNTs into silicon waveguides was studied. A laser diode emitting at a wavelength of 802 nm was used to optically pump the SWNT, in particular the (9,7) nanotube population. The incident laser beam arrived from the top of the silicon die and was focused on the silica recess, where carbon nanotubes could interact with the silicon waveguide.

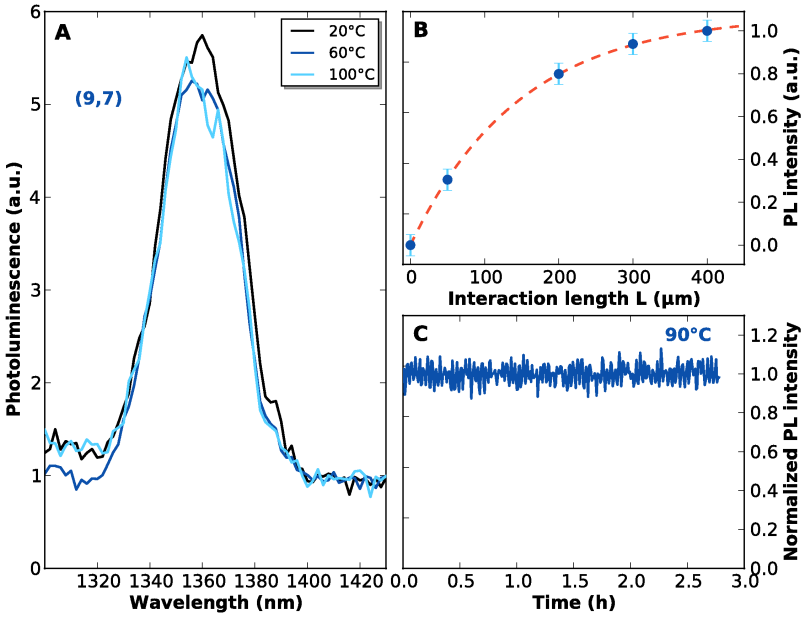

Figure 4. Coupling of carbon nanotubes PL in silicon waveguide. (A) Photoluminescence generated from the (9,7) nanotube under excitation by a 800 nm pump laser, coupled in the silicon waveguide for three temperatures (20, 60, and 100 °C). No wavelength shift or signal reduction are observed. (B) Evolution of the photoluminescence intensity as a function of the interaction waveguide length *L*. (C) Time stability of the photoluminescence coupled in the silicon waveguide at 90 °C.

The light outgoing from the output waveguide facet, placed a few millimeters away from the interaction region, was collected using a 20× microscope objective with 0.35 numerical aperture. The spectrum is displayed in Figure 4A.

This (9,7) SWNT presents a strong photoluminescence (PL) peak, at a wavelength around 1.35 μm, which is identical to the one reported in a thin PFO layer.[19] The influence of the interaction length L on the photoluminescence was also studied for several lengths between 50 and 400 μm. Results are displayed in Figure 4B. For clarity, a point with an interaction length $L = 0$ μm and PL intensity of 0 was added to the results. We noticed that the increase in PL intensity when the interaction length L increases is not linear. Indeed, its intensity increases until it reaches a maximum at L around 400 μm. This evolution could be described by a Beer−Lambert-type exponential law, meaning that the observed limitation in photoluminescence intensity is due to the SWNT/PFO layer secondary absorption. These results are consistent with previously obtained results for the absorption coupling and suggest that the optimal interaction length L_i for SWNT/PFO-based photonic devices, relying on SWNT absorption or emission properties, would be around 400 μm.

In order to furthermore determine the strength of carbon nanotubes for silicon photonic applications, we determined the SWNT emission stability with temperature. That is a major requirement for the achievement of most applications. Evolution of the (9,7) nanotube emission through the silicon waveguide is presented in Figure 4A for a given interaction length L_i of 400 μm. We notice that the SWNT PL peak did not shift in wavelength and keep the same intensity level for temperature ranging from 10 to 100 °C, which is typically the operating temperature of photonic and microelectronic systems. In order to assess thermal stability over time, PL intensity of (9,7) SWNTs was recorded for 3 h at 90 °C and is displayed in Figure 4C. The emission through the waveguide remained constant, and no thermal degradation or intensity decrease was observed.

One important point in the coupling of the photoluminescence of a 1D material such as SWNTs into the optical mode of a bulk 3D material such as a silicon waveguide is the coupling efficiency Ψ, which is the number of photons effectively transmitted through the waveguide over the total number of photons emitted by carbon nanotubes. That is

$$\Psi = \frac{N_{\text{photons transmitted}}}{N_{\text{photons emitted}}} \quad (2)$$

However, this is a very difficult task to undertake in this case. Indeed, $N_{\text{photons emitted}}$ is related to SWNT quantum yield Φ, where

$$\Phi = \frac{N_{\text{photons emitted}}}{N_{\text{photons absorbed}}} \quad (3)$$

Unfortunately, Φ is not a well-known parameter in carbon nanotubes, and it may vary greatly, in the range of 10^{-4} to 10^{-1}, depending on SWNT diameter,

surrounding, or length.[32,33] In particular, Φ is not yet determined for a PFO-embedded SWNT.

In any case, it is possible to determine the external *effective coupling factor* Q_{eff}, where

$$Q_{eff} = \Phi\Psi = \frac{N_{photons\ transmitted}}{N_{photons\ absorbed}} \quad (4)$$

Knowing the input and output power, the SWNT/PFO thin layer absorbance and the collecting setup transmission, Q_{eff} was estimated to be 2×10^{-5}.

If we estimate that the carbon nanotube quantum yield is low (*e.g.*, $\Phi = 10^{-4}$), this means that coupling efficiency Ψ is on the order of 10^{-1}. In the future, the use of photonic crystals or slot waveguides might increase the coupling between carbon nanotubes and silicon waveguides.

In light of the results obtained so far, one could state that carbon nanotube is a promising material for development of new compact and temperature-independent photonics devices on silicon.

CONCLUSIONS

In conclusion, the integration of carbon nanotube properties (absorption and photoluminescence) in silicon waveguides was studied using an integration scheme based on evanescent waveguides. The coupling of carbon nanotube photoluminescence into silicon waveguides has been demonstrated over a wide temperature range. The external effective coupling factor Q_{eff} was estimated to be about 2×10^{-5}. In the future, improved integration schemes based on photonic crystals or slot waveguides will be considered to further increase carbon nanotube coupling with photonic waveguides in order to fully exploit their extraordinary optical properties to achieve efficient optoelectronic devices in silicon.

MATERIALS AND METHODS

Carbon Nanotubes. Single-walled nanotube powder was purchased from Unydim Inc. These nanotubes were fabricated using the HiPCO process and were not purified. Poly-9,9-di-*n*-octylfluorenyl-2,7-diyl (PFO) was purchased from Sigma Aldrich. SWNT (5 mg) and PFO (5 mg) were mixed in toluene (30 mL). The mixture was homogenized, first using a water-bath sonicator for 1 h, second using a tip sonicator at 20% power for 15 min. In order to remove a part of the metallic catalyst particles from the HiPCO process and other impurities, this mixture was then centrifuged using a desktop centrifuge (typically 5−60 min at 10 000*g*). The supernatant was then collected and could be drop casted directly onto the photonics devices. The thin films were annealed at 180 °C for 15 min to improve their optical quality.

Waveguide Fabrication. Silicon-on-insulator (SOI) substrates were purchased from Soitec, with a top silicon layer of 220 nm and a buried SiO_2 layer of 1 μm. The technological steps for waveguide fabrication are as follows (see also Supporting Information S1):

- Step 1: SOI substrate preparation: cleaning with acetone under sonication, followed by O_2 plasma cleaning.
- Step 2: Waveguide definition into the e-beam resist. Deposition of 300 nm thick MaN negative resist. E-beam patterning at 20 keV, 30 s resist developing in MIF 726.
- Step 3: Pattern transfer: etching of silicon by RIE down to 6 nm thick silicon layer. RIE: SF6 (20 sccm) and O_2 (5 sccm) at 30 W for 70 s.
- Step 4: Waveguide protection by SiO_2: 500 nm thick SiO_2 layer is deposited on top of silicon waveguides at 300 °C.
- Step 5: Interaction zone definition into the e-beam resist. Deposition of 300 nm thick positive ZEP resist. E-beam patterning at 20 keV. Developing: 30 s ZED50/30 s MIBK/30 s IPA.
- Step 6: Interaction zone opening: wet etching with diluted HF of silica down to silicon stopping layer. O_2 plasma for resist removal.
- Step 7: SWNT/PFO deposition: 1 μm thick SWNT/PFO layer is deposited on the full die followed by a thermal annealing at 180 °C.
- Step 8: SWNT/PFO protection with SiO_2: 200 nm thick SiO_2 layer is deposited on top of the SWNT/PFO layer at low temperature (150 °C) to prevent layer damage.
- Step 9: Definition of protected zone into the e-beam resist. MaN resist and e-beam patterning, developing.
- Step 10: SiO_2 etching using RIE: CHF_3 (50 sccm) and O_2 (3 sccm) at 325 W (12 mTorr) for 190 s.
- Step 11: Removal of SWNT/PFO outside defined zone by RIE etching; 50% Ar and 50% O_2 at 300 W for 15 min.

Simulations. Optical simulations were performed using an homemade 2D mode solver based on the full-vectorial finite-difference method[34] and focused on anisotropic dielectric waveguides.

The filling factor $\mathcal{F}$, measure of the fraction of the mode power flux in the SWNT/PFO layer, is defined by

$$\mathcal{F} = \frac{\int^{R} P(s)\mathrm{d}s}{\int^{\infty} P(s)\mathrm{d}s}$$

where R is the SWNT/PFO layer and $P(s)$ is the mode power flux.

Determining Q_{eff}. Incoming power density on the silica recess J_i was estimated to be 2.7×10^6 W·m^2. A simple assumption is made considering the area around the waveguide whether a nanotube could interact or not. As the profile of the evanescent field is Gaussian, it is considered that the whole energy of the optical mode is confined within 5σ of the Gaussian. That is, a nanotube inside 5σ *may* interact with the waveguide, while a nanotube outside 5σ *will not* interact with the waveguide. Consequently, only the SWNT/PFO thin layer surface inside this 5σ limit will be considered. For a waveguide width W_i of 275 nm, the 5σ limit is 360 nm (*cf.* Supporting Information S2). That is, the surface area of the SWNT/PFO layer is $S_{NT} = 1.1 \times 10^{-11}$ m^2. The incident pump power on carbon nanotubes, which could couple into the waveguide, is $P_i = J_i S_{NT} = 2.91 \times 10^{-5}$ W. Absorption A of a 1 μm thick SWNT/PFO layer at 805 nm is 6.6×10^{-2} (*cf.* Supporting Information S3). Absorbed power in carbon nanotubes $P_a = AP_i = 1.92 \times 10^{-6}$ W.

On the other hand, power of the collected photoluminescence from the waveguide was $P_c = 1.27 \times 10^{-11}$ W. The collecting setup losses were estimated to be 2 dB. So the transmitted power was $P_t = P_c \times 10^{0.2} = 2.01 \times 10^{-11}$ W.

The external effective coupling factor Q_{eff} could be determined by

$$Q_{eff} = \frac{N_{photons\ transmitted}}{N_{photons\ absorbed}} = \frac{P_t/E_t}{P_a/E_a} = \frac{P_t}{P_a} \times \frac{\nu_a}{\nu_t} = \frac{P_t}{P_a} \times \frac{\lambda_t}{\lambda_a}$$

where E is the energy, ν the frequency, and λ the wavelength of the transmitted and absorbed photons.

Finally, $Q_{eff} = 1.8 \times 10^{-5} \simeq 2 \times 10^{-5}$.

Conflict of Interest: The authors declare no competing financial interest.

Acknowledgment. Authors would like to thank N. Tang from Univ. Montréal for her proofreading of the manuscript, and D. Marris-Morini and E. Cassan from Univ. Paris Sud for fruitful discussions.

Supporting Information Available: Detailed technological process of the waveguide fabrication (S1), evanescent mode profile of a 275 nm with waveguide (S2), and absorption spectra of a 1 μm thick SWNT/PFO thin layer on silica (S3). This material is available free of charge *via* the Internet at http://pubs.acs.org.

REFERENCES AND NOTES

1. Ahmed, K.; Schuegraf, K. Transistor Wars. *IEEE Spectrum* **2011**, *48*, 50–66.
2. Meindl, J. Beyond Moore's Law: The Interconnect Era. *IEEE Comput. Sci. Eng.* **2003**, *5*, 20–24.
3. Assefa, S.; Xia, F.; Green, W.; Schow, C.; Rylyakov, A.; Vlasov, Y. CMOS-Integrated Optical Receivers for On-Chip Interconnects. *IEEE J. Quantum Electron.* **2010**, *16*, 1376–1385.
4. Zalevsky, Z. Integrated Micro- and Nanophotonic Dynamic Devices: A Review. *J. Nanophotonics* **2007**, *1*, 012504.
5. Lipson, M. Guiding, Modulating, and Emitting Light on Silicon: Challenges and Opportunities. *J. Lightwave Technol.* **2005**, *23*, 4222–4238.
6. Barwicz, T.; Byun, H.; Gan, F.; Holzwarth, C.; Popovic, M.; Rakich, P.; Watts, M.; Ippen, E.; Kärtner, F.; Smith, H.; *et al.* Silicon Photonics for Compact, Energy-Efficient Interconnects. *J. Opt. Networking* **2007**, *6*, 63–73.
7. Jalali, B. Can Silicon Change Photonics? *Phys. Status Solidi A* **2008**, *205*, 213–224.
8. Liu, A.; Liao, L.; Chetrit, Y.; Basak, J.; Nguyen, H.; Rubin, D.; Paniccia, M. Wavelength Division Multiplexing Based Photonic Integrated Circuits on Silicon-on-Insulator Platform. *IEEE J. Quantum Electron.* **2010**, *16*, 23–32.
9. Lardenois, S.; Pascal, D.; Vivien, L.; Cassan, E.; Laval, S.; Orobtchouk, R.; Heitzmann, M.; Bouzaida, N.; Mollard, L. Low-Loss Submicrometer Silicon-on-Insulator Rib Waveguides and Corner Mirrors. *Opt. Lett.* **2003**, *28*, 1150–1152.
10. Fang, A.; Park, H.; Kuo, Y.-H.; Jones, R.; Cohen, O.; Liang, D.; Raday, O.; Sysak, M.; Paniccia, M.; Bowers, J. Hybrid Silicon Evanescent Devices. *Mater. Today* **2007**, *10*, 28–35.
11. Ben Bakir, B.; Descos, A.; Olivier, N.; Bordel, D.; Grosse, P.; Augendre, E.; Fulbert, L.; Fedeli, J. Electrically Driven Hybrid Si/III−V Fabry-Pérot Lasers Based on Adiabatic Mode Transformers. *Opt. Express* **2011**, *19*, 10317–10325.
12. Jurgen, M.; Jifeng, L.; Kimerling, L. High-Performance Ge-on-Si Photodetector. *Nat. Photonics* **2010**, *4*, 527–534.
13. Vivien, L.; Osmond, J.; Fedeli, J.; Marris-Morini, D.; Crozat, P.; Damlencourt, J.; Cassan, E.; Lecunff, Y.; Laval, S. 42 GHz p.i.n. Germanium Photodetector Integrated in a Silicon-on-Insulator Waveguide. *Opt. Express* **2009**, *17*, 6252–6257.
14. Reed, G.; Mashanovich, G.; Gardes, F.; Thomson, D. Silicon Optical Modulators. *Nat. Photonics* **2010**, *4*, 518–526.
15. Bachtold, A.; Hadley, P.; Nakanishi, T.; Dekker, C. Logic Circuits with Carbon Nanotube Transistors. *Science* **2001**, *294*, 1317–1320.
16. O'Connell, M.; Bachilo, S.; Huffmann, C.; Moore, V.; Strano, M.; Haroz, E.; Rialon, K.; Boul, P.; Noon, W.; Kittrell, C.; *et al.* Band Gap Fluorescence from Individual Single-Walled Carbon Nanotubes. *Science* **2002**, *297*, 593–596.
17. Bachilo, S.; Strano, M.; Kittrell, C.; Hauge, R.; Smalley, R.; Weisman, R. Structure-Assigned Optical Spectra of Single-Walled Carbon Nanotubes. *Science* **2002**, *298*, 2361–2366.
18. Nguyen, D.; Roussignol, P.; Roquelet, C.; Lauret, J.; Cassabois, G. Elastic Exciton−Exciton Scattering in Photoexcited Carbon Nanotubes. *Phys. Rev. Lett.* **2011**, *107*, 127401.
19. Gaufrès, E.; Izard, N.; Vivien, L.; Kazaoui, S.; Marris-Morini, D.; Cassan, E. Enhancement of Semiconducting Single-Wall Carbon-Nanotube Photoluminescence. *Opt. Lett.* **2009**, *34*, 3845–3847.
20. Misewich, J.; Martel, R.; Avouris, P.; Tsang, J.; Heinze, S.; Tersoff, J. Electrically Induced Optical Emission from a Carbon Nanotube FET. *Science* **2003**, *300*, 783–786.
21. Marty, L.; Adam, E.; Albert, L.; Doyon, R.; Ménard, D.; Martel, R. Exciton Formation and Annihilation during 1D Impact Excitation of Carbon Nanotubes. *Phys. Rev. Lett.* **2006**, *96*, 136803.
22. Adam, E.; Aguirre, C.; Marty, L.; St-Antoine, B.; Meunier, F.; Desjardins, P.; Ménard, D.; Martel, R. Electroluminescence from Single-Wall Carbon Nanotube Network Transistors. *Nano Lett.* **2008**, *8*, 2351–2355.
23. Weisman, R.; Bachilo, S. Dependence of Optical Transition Energies on Structure for Single-Walled Carbon Nanotubes in Aqueous Suspension: An Empirical Kataura Plot. *Nano Lett.* **2003**, *3*, 1235–1238.
24. Mueller, T.; Kinoshita, M.; Steiner, M.; Perebeinos, V.; Bol, A.; Farmer, D.; Avouris, P. Efficient Narrow-Band Light Emission from a Single Carbon Nanotube p-n Diode. *Nat. Nanotechnol.* **2009**, *5*, 27–31.
25. Gaufrès, E.; Izard, N.; Le Roux, X.; Marris-Morini, D.; Kazaoui, S.; Cassan, E.; Vivien, L. Optical Gain in Carbon Nanotubes. *Appl. Phys. Lett.* **2010**, *96*, 231105.
26. Kishida, H.; Nagasawa, Y.; Imamura, S.; Nakamura, A. Direct Observation of Dark Excitons in Micelle-Wrapped Single-Wall Carbon Nanotubes. *Phys. Rev. Lett.* **2008**, *100*, 097401.
27. Izard, N.; Gaufrès, E.; Le Roux, X.; Kazaoui, S.; Murakami, Y.; Marris-Morini, D.; Cassan, E.; Maruyama, S.; Vivien, L. Electroabsorption Study of Index-Defined Semiconducting Carbon Nanotubes. *Eur. Phys. J. Appl. Phys.* **2011**, *55*, 20401.
28. Freitag, M.; Martin, Y.; Misewich, J.; Martel, R.; Avouris, P. Photoconductivity of Single Carbon Nanotubes. *Nano Lett.* **2003**, *3*, 1067–1071.
29. St-Antoine, B.; Ménard, D.; Martel, R. Single-Walled Carbon Nanotube Thermopile for Broadband Light Detection. *Nano Lett.* **2011**, *11*, 609–613.
30. International Technology Roadmap for Semiconductors, 2009 ed., http://www.itrs.net.
31. Gaufrès, E.; Izard, N.; Le Roux, X.; Kazaoui, S.; Marris-Morini, D.; Cassan, E.; Vivien, L. Optical Microcavity with Semiconducting Single-Wall Carbon Nanotubes. *Opt. Express* **2010**, *18*, 5740–5745.
32. Berciaud, S.; Cognet, L.; Lounis, B. Luminescence Decay and the Absorption Cross Section of Individual Single-Walled Carbon Nanotubes. *Phys. Rev. Lett.* **2008**, *101*, 077402.
33. Hertel, T.; Himmelein, S.; Ackermann, T.; Stich, D.; Crochet, J. Diffusion Limited Photoluminescence Quantum Yields in 1-D Semiconductors: Single-Wall Carbon Nanotubes. *ACS Nano* **2010**, *4*, 7161–7168.
34. Fallahkhair, A.; Li, K.; Murphy, T. Vector Finite Difference Modesolver for Anisotropic Dielectric Waveguides. *J. Lightwave Technol.* **2008**, *26*, 1423–1431.